INDEXED IN
EMERGING
SOURCES
CITATION
INDEX
THOMSON REUTERS
At 2016

# Versatile drug nanocarrier assembly via conjugation of distinct carbon dots

**Yiqun Zhou,[†,1] Jiuyan Chen,[†,1] Nikolay Miloserdov,[†,1] Wei Zhang,[1] Keenan J. Mintz,[1] Braulio C. L. B. Ferreira,[1] Miodrag Micic,[2] Shanghao Li,[3] Zhili Peng,*[,4] Roger M. Leblanc*[,1]**

[1] Department of Chemistry, University of Miami, Coral Gables, FL 33146, USA

[2] Department of Engineering Design Technology, Cerritos College, Norwalk, CA 90650, USA

[3] MP Biomedicals LLC, 3 Hutton Center, Santa Ana, CA 92707, USA

[4] School of Materials Science and Engineering, Yunnan Key Laboratory for Micro/Nano Materials & Technology, Yunnan University, Kunming, Yunnan 650091, China

## Abstract

With constant emergencies and severe consequences of various central nervous system (CNS)-related diseases, drug delivery gradually reveals its significance in the modern medicine. The biggest challenge of drug delivery resides in the selection of appropriate drug delivery carrier. 21th century witnessed the prosperous development of diverse nanomaterials. Due to many excellent properties revealed in nanoscale, nanomaterials have been widely investigated as drug nanocarriers. As a new family member of carbon-based nanomaterials, carbon dots (CDs) have proved to be promising drug nanocarriers. They have been successfully conjugated with various therapeutic agents for targeted drug delivery. However, considering the limitation of single CD preparation in drug delivery, in this study, two distinct CD preparations (G-CDs and Y-CDs) were conjugated to compensate for each other's deficiencies. Different dialysis bags were employed to purify the CD conjugate (G-Y CDs) and reveal the difference between small and large-conjugated systems. After a series of physicochemical characterizations, G-Y CDs exhibited many nanocarrier-favored properties such as excitation-dependent photoluminescence (PL), diversified surface functionality, controlled morphology and versatile amphiphilicity. To further analyze the formation mechanism of G-Y CDs, self-conjugation was separately surveyed with G-CDs and Y-CDs, which showed that self-conjugation was able to occur between Y-CDs. Eventually, to evaluate the capacity of G-Y CDs as drug nanocarriers for future CNS-related diseases, G-Y CDs were intravascularly injected into the heart of zebrafish. The fluorescence signal in the spinal cord suggested the capability of G-Y CDs to cross the blood-brain barrier (BBB). Therefore, this study reveals a novel strategy to assemble versatile drug nanocarriers through conjugation of distinct CDs.

*Keywords:* Carbon dots, conjugation, characterization, drug nanocarrier

# Introduction

With the prosperous development of modern medicine, numerous diseases can be prevented, detected at early stage, managed and treated.[1-3] However, many central nervous system (CNS)-related diseases are yet a grave danger to human health, ranking the second largest cause of death.[4-6] Even though drug development for CNS-related diseases has become an urgent and focused research activity in the pharmaceutical industry,[7] the process to seek effective drugs is quite long. In addition, promising *in vitro* results don't always match the *in vivo* drug efficacy,[8] which is largely due to the presence of the blood-brain barrier (BBB).[9] The BBB prevents unrestricted leakage of substances between blood and brain in order to maintain a stable brain environment.[10, 9] Only small molecules such as water, gas and lipophilic compounds can pass the BBB through passive diffusion.[11, 12] On the other hand, the transport of large, hydrophilic or highly-charged compounds such as most drugs has to rely on specific receptor or carrier.[13, 14] Therefore, considering the presence of the BBB, only focus on drug synthesis is insufficient and unwise for the treatment of CNS-related diseases because low efficacy might result from a poor drug delivery rather than drugs themselves.[15] Drug delivery should arouse the public's attention as an equivalently important step as drug development.[16] In fact, to achieve drug delivery across the BBB, many strategies have been discovered.[17, 18] And, as a representative of the non-invasive strategy, nanoparticle (NP)-mediated drug delivery has been widely investigated with a variety of NPs used as drug nanocarriers.[19] Amongst all NP species, carbon dots (CDs) are one of the most promising drug nanocarriers.[20] As a novel class of carbon-based spherical NPs with 1-10 nm in diameter,[21] CDs were discovered by Clemson research group in 2000's.[22] Compared with gold, silver NPs, or metal-based quantum dots (QDs), CDs exhibit relatively no toxicity and high biocompatibility.[23] Compared to liposomes, CDs are smaller, which benefits the BBB penetration.[24] In contrast to carbon nanotubes, CDs are easier to synthesize with a large surface-area-to-volume ratio, which enhances the drug loading capacity.[23] CDs are also characterized for their excellent photoluminescence (PL), high water-dispersity, and tunable surface functionalities.[21] Considering their PL and water dispersity, CDs have been much applied in sensing and bioimaging *in vitro* and *in vivo*.[25] In addition, precursors and synthesis processes are tremendously important for the surface functionality of CDs. For instance, the CDs synthesized from oxygenated precursors usually have a large amount of carboxyl (-COOH) and hydroxyl groups (-OH).[26] Meanwhile, the CDs prepared with amine as a secondary reagent usually contain many primary amine groups (-NH$_2$).[20] Abundant surface functional groups endow CDs with a tunable surface to conjugate with diverse therapeutic agents.[27-29] Most importantly, except for wide distribution in the body, CDs alone or their conjugates with therapeutic agents have been constantly observed to cross the BBB with or without targeting ligands.[24] All the aforementioned properties make CDs a potent drug nanocarrier. Nevertheless, although CDs in general have abundant surface functional groups, their species and amounts for any single CD preparation are limited, which will become a big challenge to overcome in the long run of applying CDs as drug nanocarriers.[30] To date, plenty of surface modification approaches including π-π interaction, sol-gel coordination, amide coupling, silylation reaction, esterification and copolymerization have been performed to tune surface functionalities and improve the versatility of CDs for diverse applications.[31-33] After surface modification, these CDs may possess higher fluorescence quantum yield (QY), better control over the size and shape, enhanced biocompatibility and desired surface functionality.[26] However, it's yet difficult to achieve the co-existence of two dominant functional groups (-COOH and -NH$_2$) on the surface by those common surface modification strategies. Furthermore, in most cases, the surface dopants were small molecules, biomolecules and polymer linkers, and a few studies reported the conjugation of CDs with other nanomaterials.[34, 35] Nonetheless, up to now, the conjugation between distinct CDs has been rarely reported. With many excellent properties of each CD preparation taken into account, conjugation between distinct CDs might be able to centralize all these merits on the novel CD conjugate. However, due to the increase of particle size, drug delivery capacity of the CD conjugate might be harmed,

which needs to be verified with an animal model. In recent years, zebrafish (*Danio rerio*) has been widely employed as an animal model for studying human diseases such as type 2 diabetes mellitus, dyslipidemia, metabolic disorders and CNS-related diseases.[36-38] As an excellent disease model, one of the main advantages of zebrafish is its fully sequenced genome that shares high similarity with the genes associated with human diseases. In comparison to another popular animal model, namely mouse, zebrafish is smaller and cheaper to maintain in limited spaces.[39] Also, zebrafish breed at weekly intervals and can produce 50-300 eggs per time, which provides a sufficient supply of embryos and larvae for the verification of experimental results. In contrast, mice only birth 5 to 10 litters per year and each litter contains 3-14 pups.[40] Furthermore, zebrafish embryos and larvae are nearly transparent, which allows researchers to monitor the real-time development and fluorescently-labeled activities inside zebrafish.[41] On the contrary, mouse embryos are not transparent and their developments occur inside the mother. With all the differences between zebrafish and mice taken into consideration, zebrafish exhibits many advantages over mice as an *in vivo* model in this study to verify the capability of the CD conjugate to penetrate the BBB and investigate its penetration mechanism. Herein, in this study, gel-like CDs (G-CDs) and yellow CDs (Y-CDs) that originated from our group were applied as two CD models for conjugation, characterization to study the physicochemical properties of the CD conjugate (G-Y CDs), and exploration of their potential applications. Two different dialysis bags were used to acquire G-Y CDs with small and large-conjugated systems. In addition, since both G-CDs and Y-CDs have some -COOH and -NH$_2$ on the surfaces, it is necessary to discern the formation mechanism of G-Y CDs by investigating self-conjugation of G-CDs and Y-CDs. After systematic characterizations by UV/vis absorption, fluorescence emission, Fourier-transform infrared (FTIR) spectroscopies, mass spectrometry (MS), atomic force microscopy (AFM), transmission electron microscopy (TEM), thermogravimetric analysis (TGA) and zeta potential measurement, basic information of the physicochemical properties of G-Y CDs will be obtained. Moreover, the amphiphilicity of G-Y CDs will be evaluated by a solvent effect and fluorescence analysis. Moreover, because both G-CDs and Y-CDs were observed to cross the BBB and surface modifications of Y-CDs didn't affect their capability to overcome the BBB,[42, 43] G-Y CDs may be also able to penetrate the BBB, which will be investigated using a zebrafish model. Eventually, the conjugation of G-CDs and Y-CDs is expected to simultaneously introduce plenty of -NH$_2$ and -COOH to the G-Y CDs, which lays the foundation for an enhanced drug delivery for the future treatment of CNS-related diseases.

## Experimental Section

### Materials

1,2-ethylenediamine (EDA) (99.0%) was provided by MP Biomedicals (Irvine, CA, USA). 1,2-phenylenediamine (99.5%), N-(3-dimethylaminopropyl)-N′-ethylcarbodiimide hydrochloride (EDC) (97.0%) and N-hydroxysuccinimide (NHS) were purchased from Sigma-Aldrich (St Louis, MO, USA). Citric acid (99.5-100%) was acquired from VWR (West Chester, PA, USA). Compressed argon gas with ultra-high purity was ordered from Airgas (Miami, FL, USA). Size exclusion chromatography (SEC) was performed with GE Healthcare Sephacryl S-300 The deionized (DI) water used was purified using a Modulab 2020 water purification system obtained from Continental Water System Corporation. It had a pH of 6.62 ± 0.30 with surface tension and resistivity of 72.6 mN·m$^{-1}$ and 18 MΩ·cm, respectively at 25.0 ± 0.5 °C. All the chemicals were used without further treatment.

### Instrument and Methods

A Fluorolog (Horiba Jobin Yvon) spectrophotometer was used to record the fluorescence emission spectra of G-Y CDs by using a 1 cm optical cell and a slit width of 5 nm for both excitation and emission. The UV/vis absorption spectra of G-Y CDs were acquired by using a Cary 100 UV/vis spectrophotometer with a 1×1 cm optical cell. FTIR

spectroscopic data were obtained with a PerkinElmer FTIR (Frontier) spectrometer equipped by attenuated total reflection (ATR) accessories with air as background. AFM images of G-Y CDs were taken with an Agilent 5420 atomic force microscope by using the tapping mode. TEM was performed by using a JEOL 1200X transmission electron microscope. MS was performed on G-Y CDs by using a Bruker Microtof-Q in the modes of electrospray ionization (ESI) and matrix-assisted laser desorption/ionization (MALDI). Zeta potentials of G-Y CDs were measured on the Malvern Zetasizer Nano equipment, and all samples were measured at room temperature in aqueous dispersion.

### Synthesis and purification of G-Y CDs, G-G CDs and Y-Y CDs

The synthesis procedure of G-Y CDs is depicted in Figure 1. G-CDs and Y-CDs were prepared based on our previous works.[44, 45] For the synthesis of G-Y CDs, 10 mg of Y-CDs were dispersed in 4 mL PBS solution (pH 7.4) in a 100 mL round bottom flask to form Y-CD aqueous dispersion. 31.2 mg of EDC was dissolved in 2 mL PBS solution, added to the as-prepared Y-CD aqueous dispersion and stirred for 30 min. Subsequently, 18.7 mg of NHS dissolved in 2 mL PBS solution was transferred into the mixing solution and stirred for another 30 min, which was followed by the addition of 7.7 mg of G-CDs dispersed in 2 mL PBS solution and stirring overnight. The obtained sample was divided into two equal aliquots and separately purified using two different dialysis bags with molecular weight cut-off (MWCO) of 100-500 and 1000 Da against DI water for 3 days. DI water was replaced once a day. Then both dialyzed samples were collected, frozen at -80 °C and lyophilized for 2 days to acquire G-Y CD powders. For a better demonstration, samples purified with different dialysis bags are entitled G-Y CDs (100-500 Da) and (1000 Da). Later, to investigate the formation mechanism of G-Y CDs, Y-CDs and G-CDs were separately conjugated following the same synthesis and purification procedures.
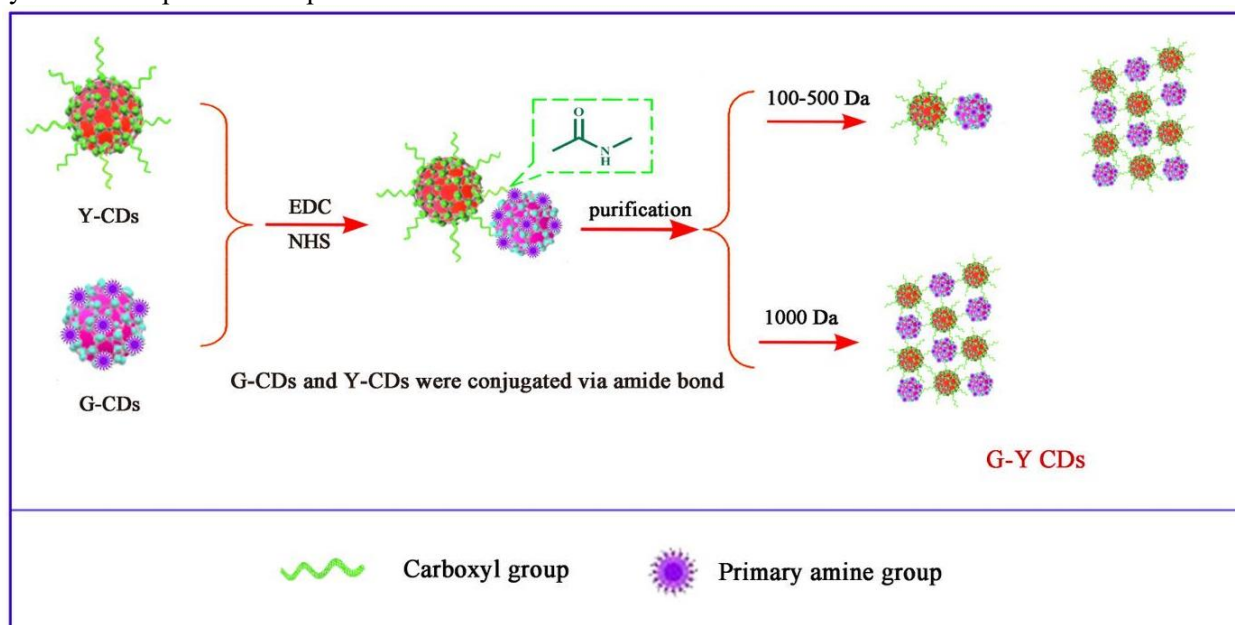


**Figure 1.** Graphical illustration of the synthesis and purification of G-Y CDs.

### Zebrafish injection and bioimaging

5-day post-fertilization (dpf) wild-type zebrafish were obtained from the Zebrafish Core Facility at University of Miami. 1 nL of aqueous dispersion (0.1 mg/µL) of each G-Y CDs (100-500 Da) and (1000 Da) were separately intravascularly injected into the heart of zebrafish that were previously anesthetized by 0.08% tricaine. After 10 min, the treated zebrafish were mounted with low-melting agar for bioimaging with a Leica SP5 confocal microscope under white light and excitation wavelength of 405 nm (for G-Y CDs). To yield robust experimental results, each test was

reproduced with 6 zebrafish. The animal care protocol for all procedures applied in this study was approved by the University of Miami Animal Care and Use Committee and complied with the guidelines of the National Science Foundation.

# Results and discussion

## *Optical properties*

The optical properties of G-Y CDs were studied using both UV/vis absorption and fluorescence emission spectroscopies. The UV/vis absorption spectra in Figure 2a show similar absorption peaks of both as-synthesized G-Y CDs (100-500 Da) and (1000 Da). They display three peaks at 233, 276 and 350 nm, which correspond to C=C, C=N and C=O conjugate structures, respectively.[46] Nonetheless, the UV/vis absorption spectra of G-Y CDs (100-500 Da) and (1000 Da) exhibit different peak intensities. The lower peak intensity of G-Y CDs (1000 Da) can be ascribed to the following reasons: 1) having the same mass concentration, G-Y CDs (1000 Da) in general own higher molecular weights, which, in turn, decreases the molar concentration; 2) due to the increase of MWCO, many small G-Y CD conjugates are filtered out. Figure 2b and 2c show the fluorescence emission and normalized spectra of G-Y CDs (100-500 Da) and (1000 Da) excited at wavelengths that range from 350 to 500 nm with an interval of 25 nm. The results demonstrate that both G-Y CDs exhibit excitation-dependent PL with the maximum excitation and emission wavelengths at 375 and 460 nm, respectively. In comparison to the fluorescence spectra of G-CDs and Y-CDs, the maximum excitation wavelength of G-Y CDs (375 nm) is between that of G-CDs (350 nm) and Y-CDs (400 nm) while the maximum emission wavelength (460 nm) is much closer to that of G-CDs (450 nm). Considering the maximum excitation wavelengths of G-CDs and Y-CDs, the maximum emission wavelengths of both G-Y CDs (100-500 Da) and (1000 Da) are compared. It turns out that the emission wavelengths of both G-Y CDs are around 450 nm under the excitation of 350 nm. However, under the excitation of 400 nm, the emission wavelength of G-Y CDs (1000 Da) is 480 nm, 20 nm longer than that of G-Y CDs (100-500 Da) and G-CDs.[44] Therefore, the overall fluorescence of G-Y CDs (100-500 Da) is dominated by that of small G-Y CD conjugates and maybe some unreacted G-CDs or Y-CDs. On the contrary, G-Y CDs (1000 Da), free from those interferences are showing fluorescence characteristics closer to that of pure but large G-Y CD conjugates.

## *Structure investigation*

ATR-FTIR was applied to investigate the functionality of G-Y CDs. From Figure 2d, the bonds at 3338-3210 cm$^{-1}$ are ascribed to O-H and/or N-H stretch vibrations that help improve the hydrophilicity of G-Y CDs.[45] The peaks at 3054-2928 cm$^{-1}$ correspond to C-H stretch vibration.[44] C-H stretch in the structure of H-C=O is shown at 2531-2208 cm$^{-1}$.[44] The peaks at 1649-1618 cm$^{-1}$ can be assigned to C=N, C=C stretch and N-H bend vibrations. Then C=O stretch vibration is observed at 1712-1687 cm$^{-1}$. C-H bend and C-C stretch vibrations in ring are observed at 1457-1375 and 1568-1532 cm$^{-1}$, respectively.[44, 46] C-N and/or C-O stretch vibrations are assigned to 1256-1241 cm$^{-1}$. However, the ATR-FTIR spectra of G-Y CDs (100-500 Da) and (1000 Da) have shown slightly different peaks. As for G-Y CDs (100-500 Da), the overall ATR-FTIR spectrum looks similar to that of free G-CDs, which confirms that in the conjugated sample of G-Y CDs (100-500 Da), there still exist a few unreacted G-CDs. In contrast, we can conclude that G-Y CDs (1000 Da) exhibit the structure of large G-Y CD conjugates and the peaks at 3054-2928 cm$^{-1}$ confirm the conjugation of G-CDs to Y-CDs in comparison with the ATR-FTIR spectrum of free Y-CDs.[47] In comparison of the MS spectra of G-Y CDs (100-500 Da) and (1000 Da) in Figure S1a and S1b, even though the same molecular ion peak (MIP) is shared by both G-Y CDs, which is 568 g/mol, the intensity of the highest ion peak of G-Y CDs (1000 Da) at 656 g/mol is much higher than that of G-Y CDs (100-500 Da). In contrast to the MS spectra of G-CDs and Y-

CDs (Figure S1c),[44] the MIPs of both G-Y CDs are close to the combination of the MIPs of free G-CDs (319 g/mol) and Y-CDs (211 g/mol), which suggests their conjugation. In addition, the difference between these two G-Y CD samples regarding the intensity of the highest ion peak indicates a higher amount of large conjugated system in G-Y CDs (1000 Da) than G-Y CDs (100-500 Da).

*Morphological features*

AFM image of G-Y CDs (100-500 Da) (Figure 2e) shows many figure-eight shaped or other simple-conjugated nanostructures. In contrast, Figure 2f shows that G-Y CDs (1000 Da) are mainly composed of large conjugated systems. The comparison between Figure 2e and 2f demonstrates that the particle size along the Z-axis of G-Y CDs is around 2 nm on average, which coincides with the mean diameters of free G-CDs or Y-CDs. Therefore, even though G-Y CDs contain large conjugated systems, the systems exhibit planar structures with a thickness of 2 nm. Meanwhile, TEM images of G-Y CDs in Figure 2g and 2h reveal many conjugated nanostructures of varying sizes. In comparison, the images demonstrate that the majority of G-Y CDs (1000 Da) are large conjugated systems while G-Y CDs (100-500 Da) contain unreacted G-CDs, Y-CDs and random conjugates of G-CDs and Y-CDs.
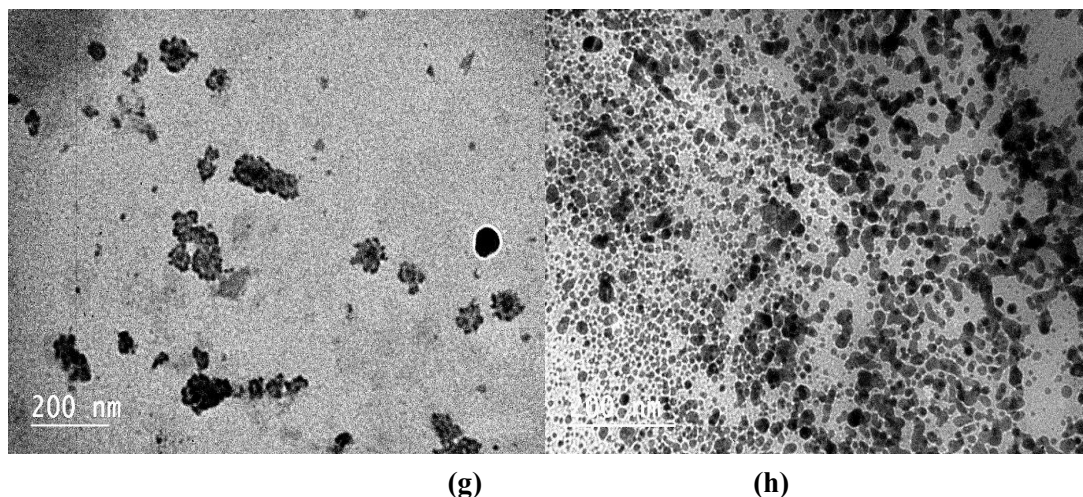
**(a)**

**(b)**

**(c)**

**(d)**

**(e)**

**(f)**

**(g)**                       **(h)**
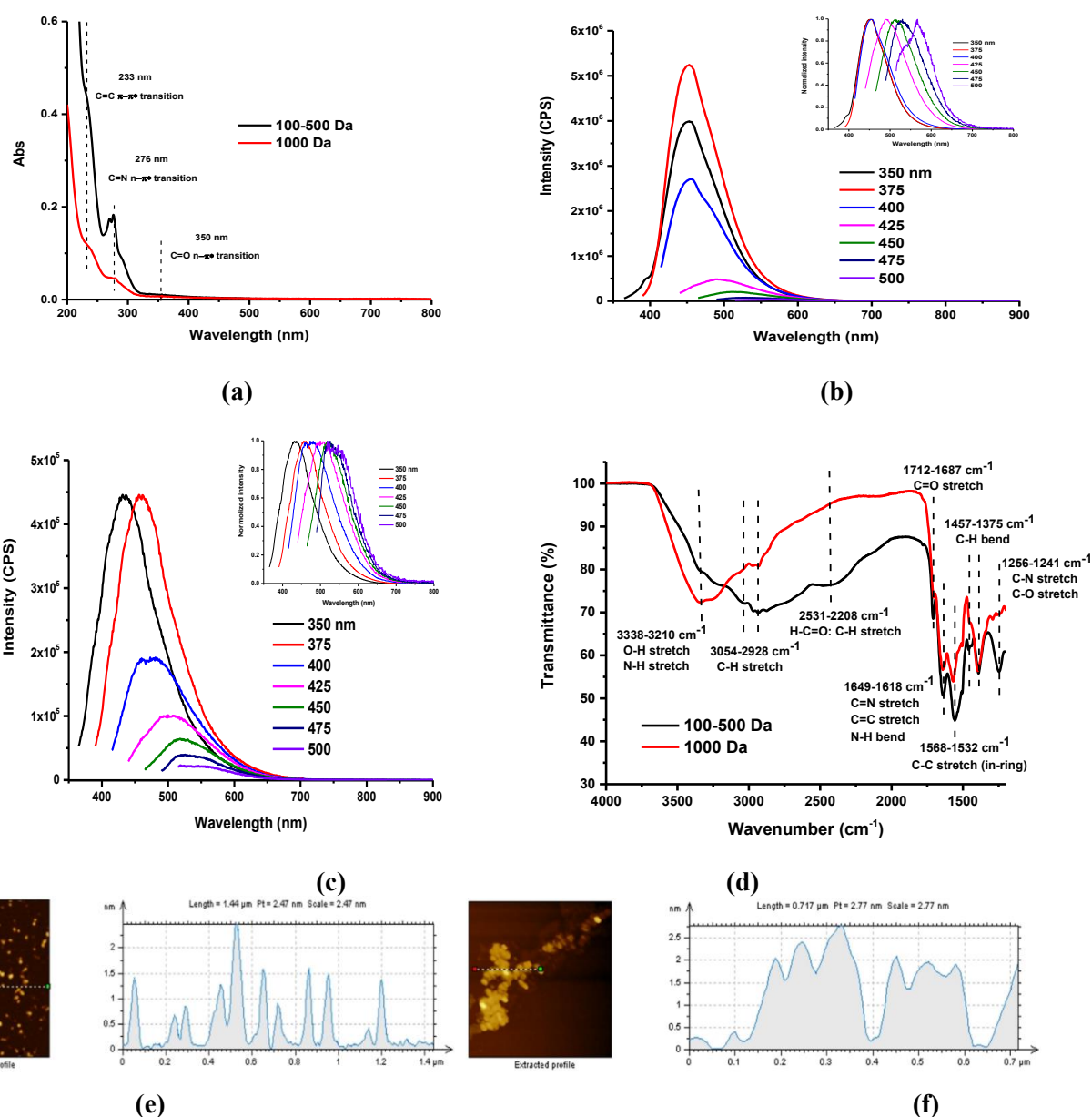
**Figure 2.** Physicochemical characterizations of G-Y CDs (100-500 Da) and (1000 Da). (a) UV/vis absorption spectra of G-Y CD aqueous dispersions (0.1 mg/mL); (b) (c) Fluorescence emission spectra of G-Y CD (100-500 Da) and (1000 Da) aqueous dispersions (0.1 mg/mL), respectively; (d) ATR-FTIR spectra with air as background; (e) (f) AFM images of G-Y CDs (100-500 Da) and (1000 Da), respectively; (g) (h) TEM images of G-Y CDs (100-500 Da) and (1000 Da), respectively.

*Amphiphilicity study*

It was observed in our previous studies that Y-CDs were amphiphilic and the amphiphilicity was not changed by surface modifications. However, G-CDs are highly hydrophilic. Therefore, in order to test if G-Y CDs are amphiphilic, 1 mg of G-Y CDs (100-500 Da) and (1000 Da) were dispersed in 10 mL water, ethanol, and acetone with a polarity index of 10.2, 4.3 and 5.1, respectively to examine their dispersity. As a result, both G-Y CDs well dispersed in water but partially dispersed in other solvents, which demonstrates a weak amphiphilicity of G-Y CDs. In addition, fluorescence emission spectra of G-Y CDs in various solvents were analyzed. In comparison among Figure 2b, 3a and 3c, a red shift is observed in the maximum emission wavelength of G-Y CDs (100-500 Da) with the increase of solvent polarity. To be specific, the maximum emission wavelength blue shifts from 450 nm (water), 435 nm (ethanol) to 430 nm (acetone). In contrast, the maximum emission spectra of G-Y CDs (1000 Da) in Figure 2c, 3b and 3d exhibit a red shift from 460 nm (water), 500 nm (ethanol) to 510 nm (acetone). Meanwhile, G-Y CDs (100-500 Da) display higher PL emission intensity in water than that in ethanol and acetone, suggesting that G-Y CDs (100-500 Da) have higher dispersity in water. However, for G-Y CDs (1000 Da), the PL emission intensity in ethanol is significantly higher than that in water and acetone, indicating a higher dispersity of G-Y CDs (1000 Da) in ethanol. Different solvent effects of G-Y CDs are a result of the use of different dialysis bags. G-Y CDs (100-500 Da) are composed of a mixture of unreacted G-CDs and random conjugates between G-CDs and Y-CDs. Even though Y-CDs have shown an excellent amphiphilicity and dispersity in various solvents with polarity-dependent PL behavior in our previous work,[45] the amphiphilicity of G-Y CDs (100-500 Da) is largely undermined by the highly hydrophilic G-CD fragment. In comparison, with high-MWCO dialysis bag, only large conjugates of G-CDs and Y-CDs were collected with the use of dialysis bag (1000 Da). And the solvent effect of G-Y CDs (1000 Da) will be less interfered by impurities. Instead, as was reported in our previous study, surface modification won't change the amphiphilicity of Y-CDs. Therefore, the solvent effect of G-Y CDs (1000 Da) tends to be closer to that of Y-CDs.
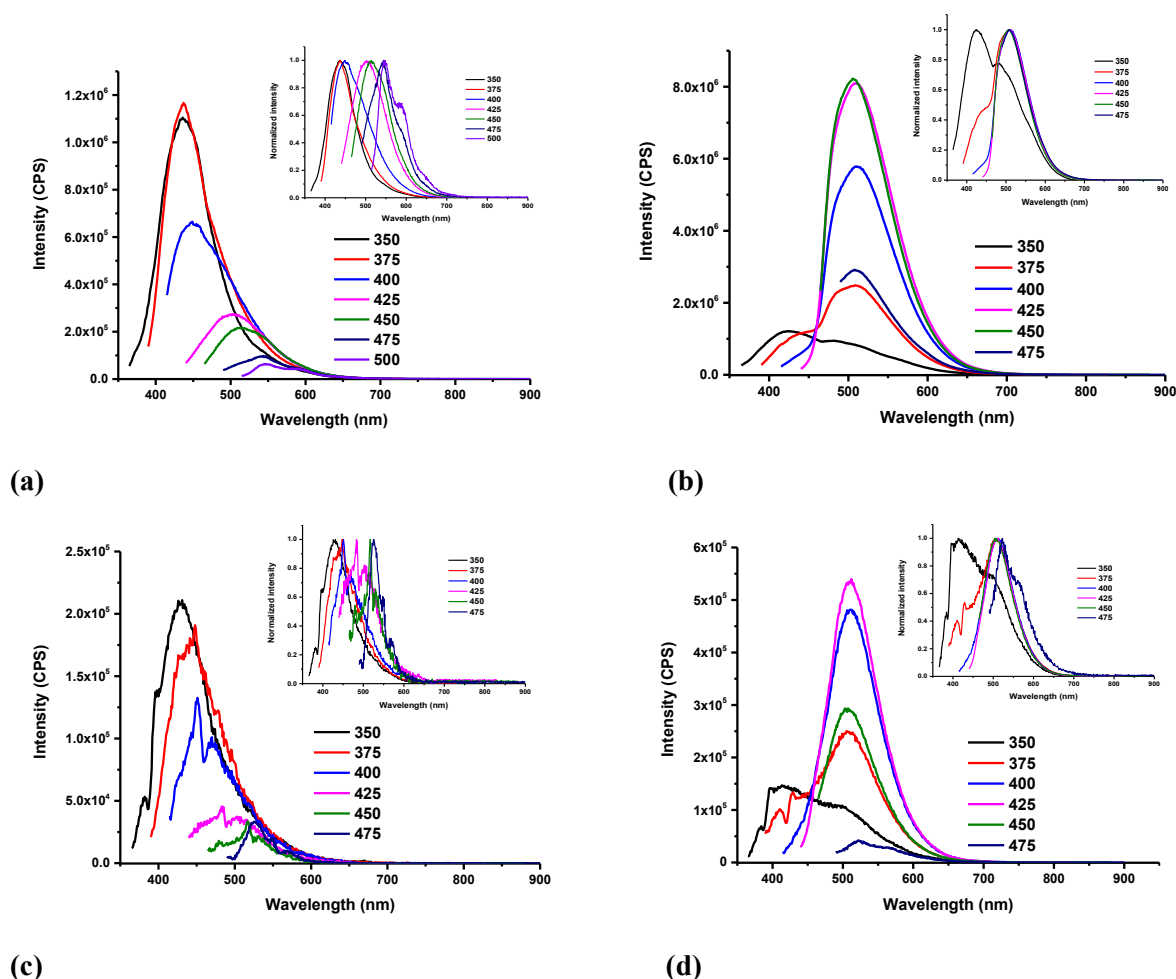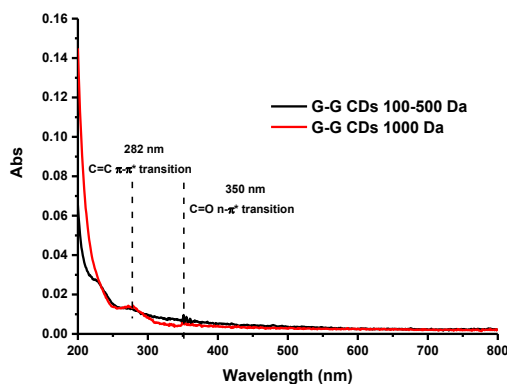
**Figure 3.** Fluorescence emission spectra of 1 mg of G-Y CDs (100-500 Da) and (1000 Da) dispersed in 10 mL different organic solvents. (a) (b) G-Y CDs (100-500 Da) and (1000 Da) in ethanol, respectively; (c) (d) G-Y CDs (100-500 Da) and (1000 Da) in acetone, respectively.

### *Formation mechanism of G-Y CDs*

According to our previous work, Y-CDs were characterized with appreciable amount of -COOH and a few -NH$_2$.[47] In contrast, the predominant functionality of G-CDs is -NH$_2$.[48] Theoretically, when -COOH on Y-CDs are activated and stabilized by EDC and NHS, respectively, Y-CDs can be conjugated to G-CDs via an amidation reaction. However, considering the presence of both -COOH and -NH$_2$ on each CDs, to investigate the formation mechanism of G-Y CDs and explore if G-CDs and Y-CDs can self-conjugate, G-CDs and Y-CDs were separately conjugated following the same methodologies as G-Y CDs. UV/vis absorption spectra in Figure 4a exhibit absorption peaks at 282 and 350 nm that are similar to the UV/vis absorption spectrum of free G-CDs in our previous work.[44] In addition, fluorescence analyses of G-G conjugated samples in Figure 4c and Figure 4d display an excitation-dependent PL emission with the same maximum excitation and emission wavelengths of free G-CDs.[48] As for the possible formation of Y-Y CDs, only two peaks ascribed to C=C (~230 nm) and C=O (~285 nm) are shown in the spectra of Y-Y conjugated samples (Figure 4b), which is different from that of free Y-CDs with four absorption peaks at C=C (235 nm), C=N (255 nm), C=O (285 nm) and low-energy region (421 nm).[47] It suggests that Y-CDs might self-conjugate. It was further confirmed by the excitation-dependent PL emission of Y-Y CDs (1000 Da) with the maximum excitation and emission wavelengths at 450 and 530 nm, respectively. In comparison to those of free Y-CDs, the maximum emission occurred blue shift. In contrast, even though Y-Y CDs (100-500 Da) also exhibited excitation-dependent PL, the

emission spectrum in Figure 4f seems to be composed of two fluorescence centers, which demonstrates the impurity of Y-Y CDs (100-500 Da). Further evidence of conjugation was provided by ATR-FTIR spectra of G-G conjugated samples and Y-Y CDs. All the peaks share by free G-CDs and G-G conjugated samples exclude the possible G-G CD conjugation from G-Y CDs. Meanwhile, varied peaks of Y-Y CDs demonstrate the successful self-conjugation of Y-CDs as well as the control of MWCO of dialysis bag over the purity and uniformity of CD conjugates. Furthermore, the self-conjugation was also confirmed by the TEM image (Figure 4i) of Y-Y CDs (1000 Da) with relatively uniform spherical shape and size (68.31±30.62 nm).
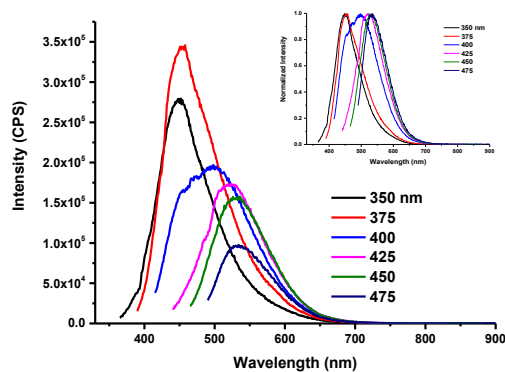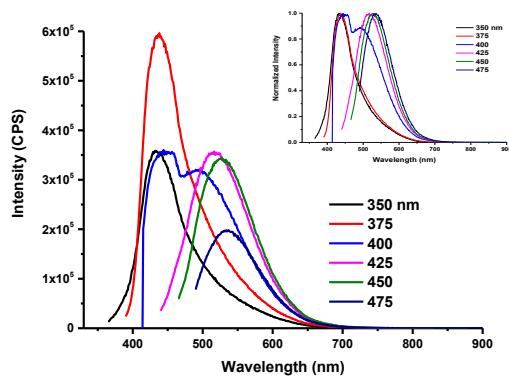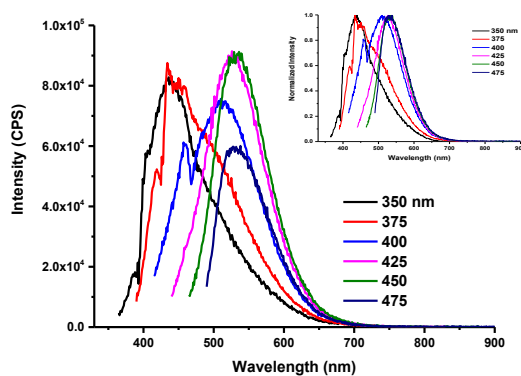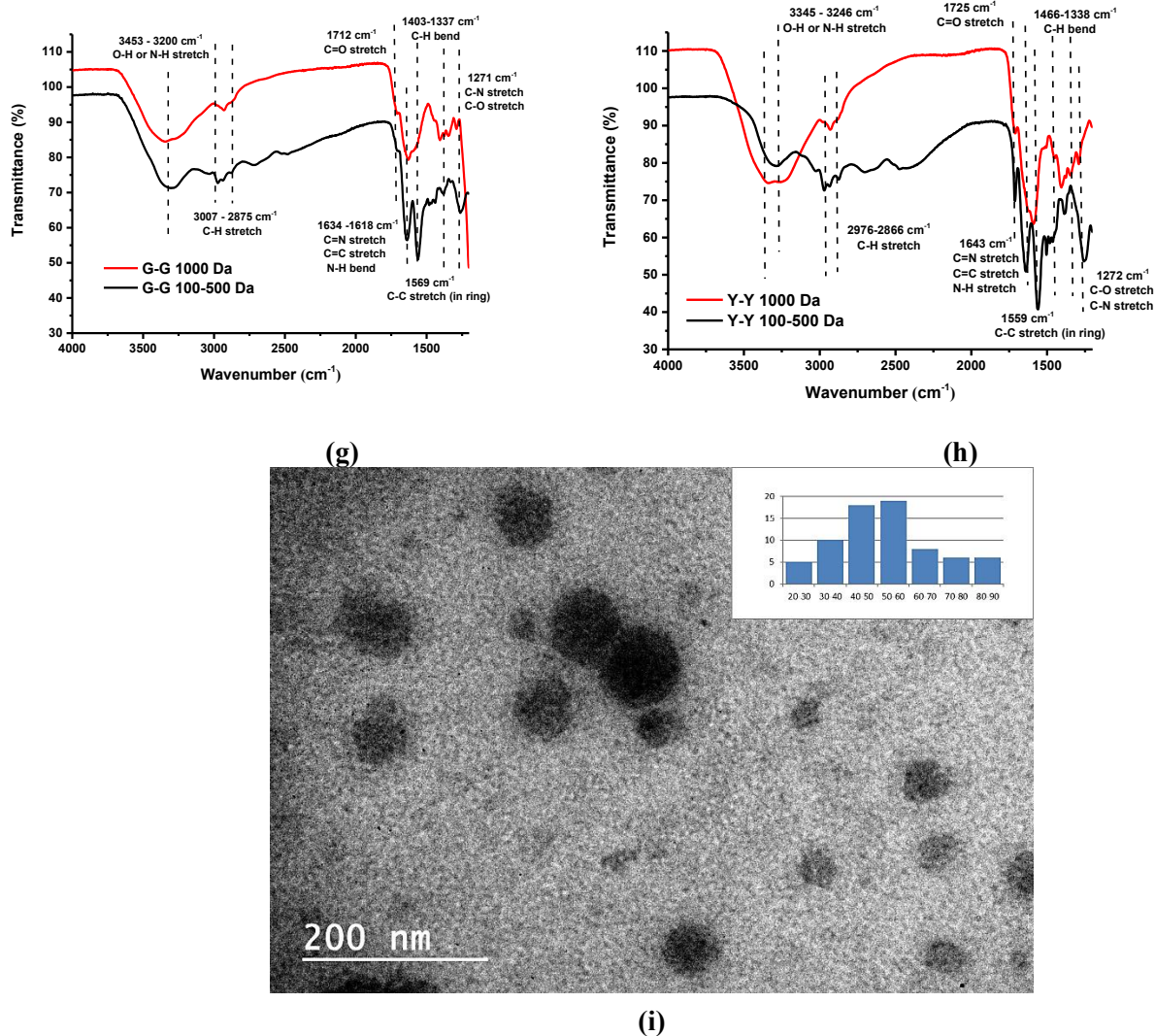


(a)



(b)



(c)



(d)



(e)



(f)

**(g)**

**(h)**



**(i)**
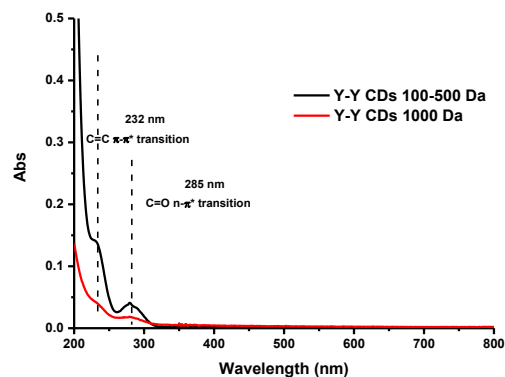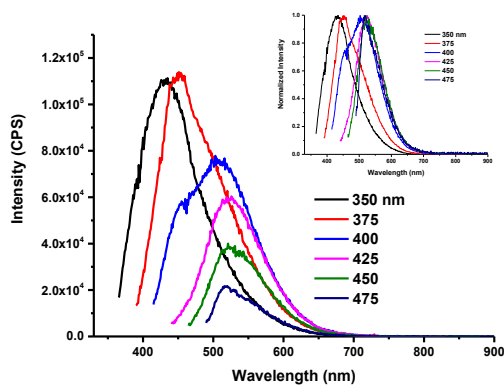
**Figure 4.** Physicochemical characterizations of G-G conjugated samples and Y-Y CDs (100-500 Da) and (1000 Da). (a) (b) UV/vis absorption spectra of G-G conjugated samples and Y-Y CDs (0.1 mg/mL), respectively; (c) (d) Fluorescence emission spectra of possible G-G conjugated samples (100-500 Da) and (1000 Da) (0.1 mg/mL), respectively; (e) (f) Fluorescence emission spectra of Y-Y CDs (100-500 Da) and (1000 Da) (0.1 mg/mL), respectively; (g) (h) ATR-FTIR spectra of G-G conjugated sample and Y-Y CDs, respectively with air as background; (i) TEM image of Y-Y CDs (1000 Da).

### *Zebrafish bioimaging*

It was discovered that 70% of genes related to human diseases have functional homologs in zebrafish.[49] Thus, zebrafish has become one of the most popular animal models to study developmental processes and human disorders.[50, 51] Specifically, zebrafish were frequently applied in CNS disorder studies: 1) as a model system for the treatment of Alzheimer's and Parkinson's diseases;[52, 53] 2) seeking neuroactive drugs through behavioral screening.[54, 55] Due to the unpredictability when relating *in vitro* studies to *in vivo* experiments, the use of animal models such as zebrafish gets more and more necessary. To investigate whether G-Y CDs can penetrate the BBB, 0.1 mg/µL aqueous dispersions of G-Y CDs (100-500 Da) and (1000 Da) were separately injected into the heart of zebrafish. Under the excitation of 405 nm, the fluorescence signals shown in the central canal of spinal cord (Figure 5) demonstrate that both G-Y CDs (100-500 Da) and (1000 Da) are able to overcome the BBB in comparison to the control. As to the BBB penetration mechanism of G-Y CDs, the best explanation is passive diffusion. First of all, the precursors of G-CDs and Y-CDs don't contain transferrin or folic acid, whose receptors are overexpressed on the BBB. And since the

precursors were not tryptophan or glucose that could overcome the BBB with unique transport proteins. Thus, G-Y CDs across the BBB could not be caused by a receptor-mediated endocytosis or carrier-mediated transport. Furthermore, considering the zeta potentials of -6.45±0.86 and -22.90±1.12 mV for G-Y CDs (100-500 Da) and (1000 Da), respectively, the BBB penetration of G-Y CDs unlikely undergoes adsorption-mediated endocytosis. Instead, the low zeta potential values confirm the amphiphilicity of G-Y CDs and ensure G-Y CDs across the basement membrane of the BBB. Moreover, different zeta potentials demonstrate that G-Y CDs (1000 Da) have a higher aqueous stability in comparion to G-Y CDs (100-500 Da) due to their composition.
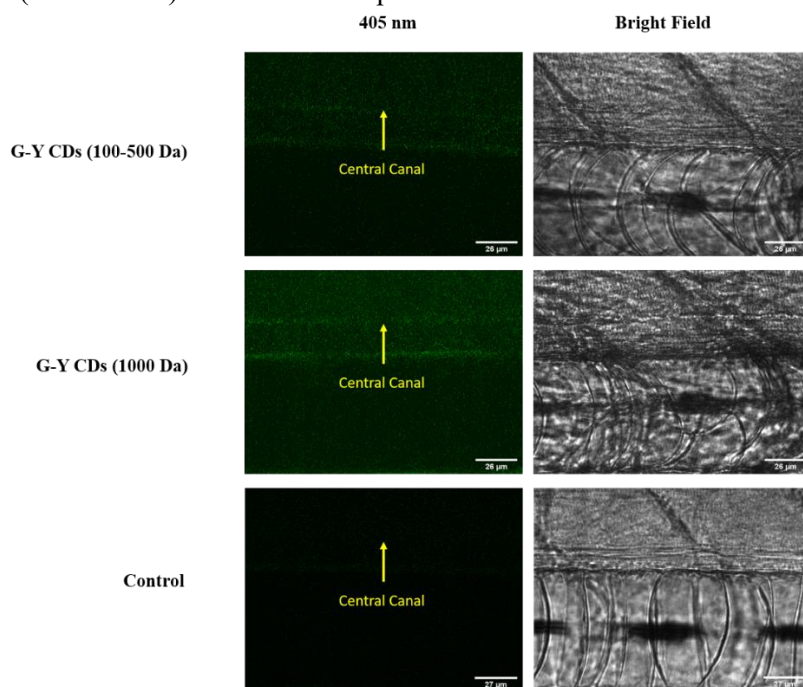


**Figure 5.** Confocal images of zebrafish treated with G-Y CDs (0.1 mg/µL) with control.

## Conclusions

In order to acquire a versatile drug nanocarrier for the treatment of various CNS-related diseases, two distinct types of CDs were conjugated and studied for their physicochemical and biological properties. In order to compare small and large-conjugated systems, two different dialysis bags were employed to purify the obtained G-Y CDs. In comparison to the G-Y CDs (100-500 Da), G-Y CDs (1000 Da) were retained with unique optical properties, structure and morphology. Most significantly, through conjugation, the novel conjugated nanostructure obtains abundant -COOH and -NH$_2$, which is of great benefit for future drug delivery. In addition, the novel G-Y CDs are amphiphilic due to the presence of Y-CD fragment in the conjugated structure, which will play an important role in overcoming cell membranes and various barriers present in human body. To investigate the formation mechanism of G-Y CDs, G-CDs and Y-CDs were conjugated for trial and Y-CDs have shown the capability to self-conjugate, which suggests the conjugation pattern between G-CDs and Y-CDs is not 1:1. Eventually, when both G-Y CDs were intravascularly injected into the heart of zebrafish, both CDs were observed to cross the BBB via passive diffusion. In general, the successful conjugation between G-CDs and Y-CDs demonstrates the possibility of accumulating all the advantages of individual CD on one novel nanostructure for drug delivery. It indicates the beginning of utilizing CDs as Lego-like building blocks for the assembly of various large structures for diverse applications.

**References**

1. Smith RD. Responding to global infectious disease outbreaks: lessons from SARS on the role of risk perception, communication and management. *Soc. Sci. Med*. 2006; 63: 3113-3123.

2. Bleakley H. Disease and Development: Evidence from Hookworm Eradication in the American South*. *Q. J. Econ*. 2007; 122: 73-117.

3. Qian Z, Chai L, Tang C, Huang Y, Chen J and Feng H. A fluorometric assay for acetylcholinesterase activity and inhibitor screening with carbon quantum dots. *Sensor. Actuat. B*. 2016; 222: 879-886.

4. Barnholtz-Sloan JS, Sloan AE, Davis FG, Vigneau FD, Lai P and Sawaya RE. Incidence proportions of brain metastases in patients diagnosed (1973 to 2001) in the Metropolitan Detroit Cancer Surveillance System. *J. Clin. Oncol.* 2004; 22: 2865-2872.

5. Spindler KR and Hsu T-H. Viral disruption of the blood–brain barrier. *Trends Microbiol.* 2012; 20: 282-290.

6. Siegel R, Ma J, Zou Z and Jemal A. Cancer statistics, 2014. *CA Cancer J. Clin.* 2014; 64: 9-29.

7. Chandler DJ. Something's got to give: psychiatric disease on the rise and novel drug development on the decline. *Drug Discov. Today.* 2013; 18: 202-206.

8. Mak IW, Evaniew N and Ghert M. Lost in translation: animal models and clinical trials in cancer treatment. *Am. J. Transl. Res*. 2014; 6: 114-118.

9. Pardridge WM. The blood-brain barrier: bottleneck in brain drug development. *NeuroRX*. 2005; 2: 3-14.

10. Banks WA. Diseases mediated by the BBB. *Handbook of Biologically Active Peptides*. 2013, p. 1667-1671.

11. Abbott NJ, Rönnbäck L and Hansson E. Astrocyte–endothelial interactions at the blood–brain barrier. *Nat. Rev. Neurosci*. 2006; 7: 41-53.

12. Harati R, Villégier A-S, Banks WA and Mabondzo A. Susceptibility of juvenile and adult blood–brain barrier to endothelin-1: regulation of P-glycoprotein and breast cancer resistance protein expression and transport activity. *J. Neuroinflammation.* 2012; 9: 273-288.

13. Shen DD, Artru AA and Adkison KK. Principles and applicability of CSF sampling for the assessment of CNS drug delivery and pharmacodynamics. *Adv. Drug Deliv. Rev.* 2004; 56: 1825-1857.

14. Zheng W, Aschner M and Ghersi-Egea J-F. Brain barrier systems: a new frontier in metal neurotoxicological research. *Toxicol. Appl. Pharmacol.* 2003; 192: 1-11.

15. Gaillard PJ, Visser CC, Appeldoorn CCM and Rip J. Enhanced brain drug delivery: safely crossing the blood–brain barrier. *Drug Discov. Today Technol.* 2012; 9: e155-e160.

16. Allen TM and Cullis PR. Drug delivery systems: entering the mainstream. *Science*. 2004; 303: 1818-1822.

17. Gumerlock MK, Belshe BD, Madsen R and Watts C. Osmotic blood-brain barrier disruption and chemotherapy in the treatment of high grade malignant glioma: patient series and literature review. *J. Neuro-Oncol*. 1992; 12: 33-46.

18. Wu S-K, Chu P-C, Chai W-Y, et al. Characterization of different microbubbles in assisting focused ultrasound-

induced blood-brain barrier opening. *Sci. Rep*. 2017; 7: 46689-46699.

19. Ahlawat J, Guillama Barroso G, Masoudi Asil S, et al. Nanocarriers as potential drug delivery candidates for overcoming the blood–brain barrier: challenges and possibilities. *ACS Omega*. 2020; 5: 12583-12595.

20. Peng Z, Miyanji EH, Zhou Y, et al. Carbon dots: promising biomaterials for bone-specific imaging and drug delivery. *Nanoscale*. 2017; 9: 17533-17543.

21. Zhou Y, Mintz KJ, Sharma SK and Leblanc RM. Carbon dots: diverse preparation, application, and perspective in surface chemistry. *Langmuir*. 2019; 35: 9115-9132.

22. Riggs JE, Guo Z, Carroll DL and Sun Y-P. Strong luminescence of solubilized carbon nanotubes. *J. Am. Chem. Soc.* 2000; 122: 5879-5880.

23. Hettiarachchi SD, Zhou Y, Seven E, et al. Nanoparticle-mediated approaches for Alzheimer's disease pathogenesis, diagnosis, and therapeutics. *J. Control. Release.* 2019; 314: 125-140.

24. Zhou Y, Peng Z, Seven ES and Leblanc RM. Crossing the blood-brain barrier with nanoparticles. *J. Control. Release.* 2018; 270: 290-303.

25. Peng H and Travas-Sejdic J. Simple aqueous solution route to luminescent carbogenic dots from carbohydrates. *Chem. Mater*. 2009; 21: 5563-5565.

26. Yan F, Jiang Y, Sun X, Bai Z, Zhang Y and Zhou X. Surface modification and chemical functionalization of carbon dots: a review. *Microchim. Acta*. 2018; 185: 424-457.

27. Sarkar S, Das K and Das PK. Estradiol hemisuccinate-modified surface-engineered carbon dots: target-specific theranostic agent. *ACS Sustain. Chem. Eng.* 2017; 5: 8356-8369.

28. Ding C, Zhu A and Tian Y. Functional surface engineering of c-dots for fluorescent biosensing and in vivo bioimaging. *Acc. Chem. Res.* 2014; 47: 20-30.

29. Pandit S, Behera P, Sahoo J and De M. In situ synthesis of amino acid functionalized carbon dots with tunable properties and their biological applications. *ACS Appl. Bio Mater.* 2019; 2: 3393-3403.

30. Li S, Wang L, Chusuei CC, et al. Nontoxic carbon dots potently inhibit human insulin fibrillation. *Chem. Mater*. 2015; 27: 1764-1771.

31. Yang F, LeCroy GE, Wang P, et al. Functionalization of carbon nanoparticles and defunctionalization—toward structural and mechanistic elucidation of carbon "quantum" dots. *J. Phys. Chem. C*. 2016; 120: 25604-25611.

32. Srivastava I, Misra SK, Bangru S, et al. Complementary oligonucleotide conjugated multicolor carbon dots for intracellular recognition of biological events. *ACS Appl. Mater. Interfaces.* 2020; 12: 16137-16149.

33. Sarma D, Majumdar B and Sarma TK. Carboxyl-functionalized carbon dots as competent visible light photocatalysts for aerobic oxygenation of alkyl benzenes: role of surface functionality. *ACS Sustain. Chem. Eng*. 2018; 6: 16573-16585.

34. Wen Y, Xu M, Liu X, et al. Magnetofluorescent nanohybrid comprising polyglycerol grafted carbon dots and iron oxides: colloidal synthesis and applications in cellular imaging and magnetically enhanced drug delivery. *Colloids Surf. B*. 2019; 173: 842-850.

35. Wang Y, Zhang C, Chen X, et al. Ratiometric fluorescent paper sensor utilizing hybrid carbon dots-quantum dots for the visual determination of copper ions. *Nanoscale*. 2016; 8: 5977-5984.

36. Basu S and Sachidanandan C. Zebrafish: a multifaceted tool for chemical biologists. *Chem. Rev*. 2013; 113: 7952-7980.

37. Suen MFK, Chan WS, Hung KWY, Chen YF, Mo ZX and Yung KKL. Assessments of the effects of nicotine and ketamine using tyrosine hydroxylase-green fluorescent protein transgenic zebrafish asbiosensors. *Biosens. Bioelectron.* 2013; 42: 177-185.

38. Nishimura Y, Yata K, Nomoto T, et al. Identification of a novel indoline derivative for in vivo fluorescent imaging of blood-brain barrier disruption in animal models. *ACS Chem. Neurosci.* 2013; 4: 1183-1193.

39. Li S, Peng Z, Dallman J, et al. Crossing the blood–brain–barrier with transferrin conjugated carbon dots: a zebrafish model study. *Colloids Surf. B.* 2016; 145: 251-256.

40. Westerfield M. The zebrafish book 4th ed. Univ. of Oregon Press, Eugene, 2000.

41. Meyers JR. Zebrafish: development of a vertebrate model organism. *Curr. Protoc*. 2018; 16: e19-e44.

42. Hettiarachchi SD, Graham RM, Mintz KJ, et al. Triple conjugated carbon dots as a nano-drug delivery model for glioblastoma brain tumors. *Nanoscale*. 2019; 11: 6192-6205.

43. Zhou Y, Liyanage PY, Geleroff DL, et al. Photoluminescent Carbon dots: a mixture of heterogeneous fractions. *Chemphyschem*. 2018; 19: 2589-2597.

44. Zhou Y, Desserre A, Sharma SK, et al. Gel-like carbon dots: characterization and their potential applications. 2017; 18: 890-897.

45. Zhou Y, Mintz KJ, Oztan CY, et al. Embedding carbon dots in superabsorbent polymers for additive manufacturing. 2018; 10: 921-932.

46. Zhou Y, Zahran EM, Quiroga BA, et al. Size-dependent photocatalytic activity of carbon dots with surface-state determined photoluminescence. *Appl. Catal. B.* 2019; 248: 157-166.

47. Zhou Y, Liyanage PY, Devadoss D, et al. Nontoxic amphiphilic carbon dots as promising drug nanocarriers across the blood–brain barrier and inhibitors of β-amyloid. *Nanoscale*. 2019; 11: 22387-22397.

48. Zhou Y, Mintz KJ, Cheng L, et al. Direct conjugation of distinct carbon dots as Lego-like building blocks for the assembly of versatile drug nanocarriers. *J. Colloid Interface Sci.* 2020; 576: 412-425.

49. Langheinrich U. Zebrafish: a new model on the pharmaceutical catwalk. *Bioessays*. 2003; 25: 904-912.

50. Rudner LA, Brown KH, Dobrinski KP, et al. Shared acquired genomic changes in zebrafish and human T-ALL. *Oncogene*. 2011; 30: 4289-4296.

51. Outtandy P, Russell C, Kleta R and Bockenhauer DJPN. Zebrafish as a model for kidney function and disease. *Pediatr. Nephrol*. 2019; 34: 751-762.

52. Xi Y, Noble S, Ekker MJCN and Reports N. Modeling neurodegeneration in zebrafish. *Curr. Neurol. Neurosci. Rep.* 2011; 11: 274-282.

53. Saleem S and Kannan RR. Zebrafish: an emerging real-time model system to study Alzheimer's disease and neurospecific drug discovery. *Cell Death Discov*. 2018; 4: 45-57.

54. Kokel D, Bryan J, Laggner C, et al. Rapid behavior-based identification of neuroactive small molecules in the zebrafish. *Nat. Chem. Biol.* 2010; 6: 231-237.

55. Rihel J, Prober DA, Arvanites A, et al. Zebrafish behavioral profiling links drugs to biological targets and rest/wake regulation. *Science.* 2010; 327: 348-351.